The V-type ATPase enhances photosynthesis in marine phytoplankton and further links phagocytosis to symbiogenesis

Daniel P Yee, Ty J Samo, Raffaela M Abbriano, Bethany Shimasaki, Maria Vernet, Xavier Mayali, Peter K Weber, B. Greg Mitchell, Mark Hildebrand, Johan Decelle, et al.

Report

Current Biology

The V-type ATPase enhances photosynthesis in marine phytoplankton and further links phagocytosis to symbiogenesis

Graphical abstract

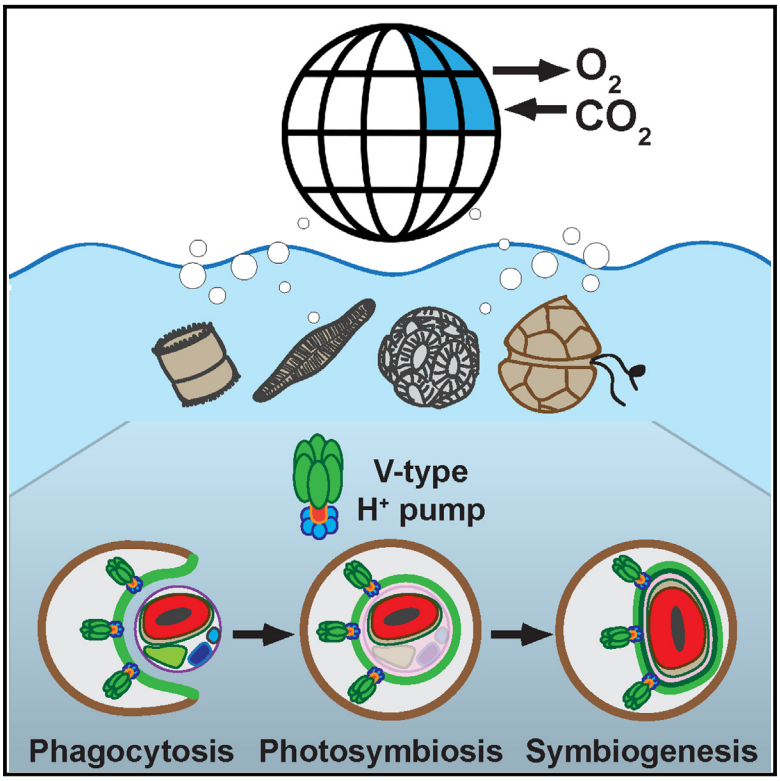

Highlights

- The V-type H^+-ATPase (VHA) promotes photosynthesis in secondary endosymbiotic algae
- VHA around diatom plastids contributes to the carbon-concentrating mechanism (CCM)
- This VHA-mediated CCM generates at least 7% of the primary production in the ocean
- Similar VHA-CCMs in extant photosymbioses are a selectable trait for symbiogenesis

Authors

Daniel P. Yee, Ty J. Samo, Raffaela M. Abbriano, ..., Mark Hildebrand, Johan Decelle, Martin Tresguerres

Correspondence

daniel.p.yee@gmail.com (D.P.Y.), mtresguerres@ucsd.edu (M.T.)

In brief

Yee et al. show that a proton pump in endosymbiotic membranes around chloroplasts of secondary endosymbiotic algae contributes to a carbon-concentrating mechanism that enhances photosynthesis. Evolution of a similar mechanism in the digestive membranes of other photosymbiotic taxa provides functional evidence for phagocytosis-derived symbiogenesis.

Yee et al., 2023, Current Biology *33*, 2541–2547
June 19, 2023
https://doi.org/10.1016/j.cub.2023.05.020

CellPress

Current Biology

CellPress
OPEN ACCESS

Report

The V-type ATPase enhances photosynthesis in marine phytoplankton and further links phagocytosis to symbiogenesis

Daniel P. Yee,[1,3,4,6,*] Ty J. Samo,[2] Raffaela M. Abbriano,[1] Bethany Shimasaki,[1] Maria Vernet,[1] Xavier Mayali,[2] Peter K. Weber,[2] B. Greg Mitchell,[1] Mark Hildebrand,[1] Johan Decelle,[3] and Martin Tresguerres[1,5,*]

[1]Scripps Institution of Oceanography, University of California San Diego, 9500 Gilman Drive, La Jolla, CA 92093, USA
[2]Physical and Life Sciences Directorate, Lawrence Livermore National Laboratory, 7000 East Avenue, Livermore, CA 94550, USA
[3]Cell and Plant Physiology Laboratory, University of Grenoble Alpes, CNRS, CEA, INRAE, and IRIG, 17 Avenue des Martyrs, Grenoble 38054, Auvergne-Rhone-Alpes, France
[4]Twitter: @DanielPYee
[5]Twitter: @martin3guerres
[6]Lead contact
*Correspondence: daniel.p.yee@gmail.com (D.P.Y.), mtresguerres@ucsd.edu (M.T.)
https://doi.org/10.1016/j.cub.2023.05.020

SUMMARY

Diatoms, dinoflagellates, and coccolithophores are dominant groups of marine eukaryotic phytoplankton that are collectively responsible for the majority of primary production in the ocean.[1] These phytoplankton contain additional intracellular membranes around their chloroplasts, which are derived from ancestral engulfment of red microalgae by unicellular heterotrophic eukaryotes that led to secondary and tertiary endosymbiosis.[2] However, the selectable evolutionary advantage of these membranes and the physiological significance for extant phytoplankton remain poorly understood. Since intracellular digestive vacuoles are ubiquitously acidified by V-type H^+-ATPase (VHA),[3] proton pumps were proposed to acidify the microenvironment around secondary chloroplasts to promote the dehydration of dissolved inorganic carbon (DIC) into CO_2, thus enhancing photosynthesis.[4,5] We report that VHA is localized around the chloroplasts of centric diatoms and that VHA significantly contributes to their photosynthesis across a wide range of oceanic irradiances. Similar results in a pennate diatom, dinoflagellate, and coccolithophore, but not green or red microalgae, imply the co-option of phagocytic VHA activity into a carbon-concentrating mechanism (CCM) is common to secondary endosymbiotic phytoplankton. Furthermore, analogous mechanisms in extant photosymbiotic marine invertebrates[6–8] provide functional evidence for an adaptive advantage throughout the transition from endosymbiosis to symbiogenesis. Based on the contribution of diatoms to ocean biogeochemical cycles, VHA-mediated enhancement of photosynthesis contributes at least 3.5 Gtons of fixed carbon per year (or 7% of primary production in the ocean), providing an example of a symbiosis-derived evolutionary innovation with global environmental implications.

RESULTS AND DISCUSSION

VHA contribution to O_2 production by marine microalgae

To test if VHA plays a functional role in phytoplankton photosynthesis, we measured O_2 production in multiple marine microalgae exposed to concanamycin A (10 nM), a highly specific inhibitor of VHA in all eukaryotes (Figure S1), which, at nanomolar concentrations, does not affect ATPase synthase or P-type ATPases.[9–14] Inhibition of VHA significantly decreased gross O_2 production in exponentially growing cultures of the centric diatom *Thalassiosira pseudonana* (~20% inhibition), the pennate diatom *Phaeodactylum tricornutum* (~16%), the dinoflagellate *Brandtodinium nutricula* (~20%), and the coccolithophore *Emiliania huxleyi* (~40%) (Figure 1; Table S1). In contrast, concanamycin A did not affect O_2 production in the primary endosymbiotic green and red alga, *Chlorella prototheocoides* and *Porphyridium purpureum*, respectively (Figure 1; Table S1). Although these algae do possess VHA that contributes to vacuole homeostasis and cytosolic pH regulation,[15–17] their chloroplasts lack the additional membranes that are typical of secondary and tertiary endosymbiotic phytoplankton. Thus, the inhibitory effect of concanamycin A on O_2 production in diatoms, dinoflagellates, and coccolithophores is likely due to inhibition of VHA in the additional membranes of phagocytic origin that surround their chloroplasts.

Expression and subcellular localization of VHA in *T. pseudonana*

We further explored this putative VHA-mediated mechanism in *T. pseudonana*, a model diatom that can be cell cycle synchronized by silicon starvation and re-addition to produce cultures containing cells in semi-homogeneous physiological conditions.[18] The VHA is a holoenzyme protein complex that is composed of 16 subunits, with a membrane spanning V_0-domain and cytosolic facing catalytic V_1-domain (Figure 2A).

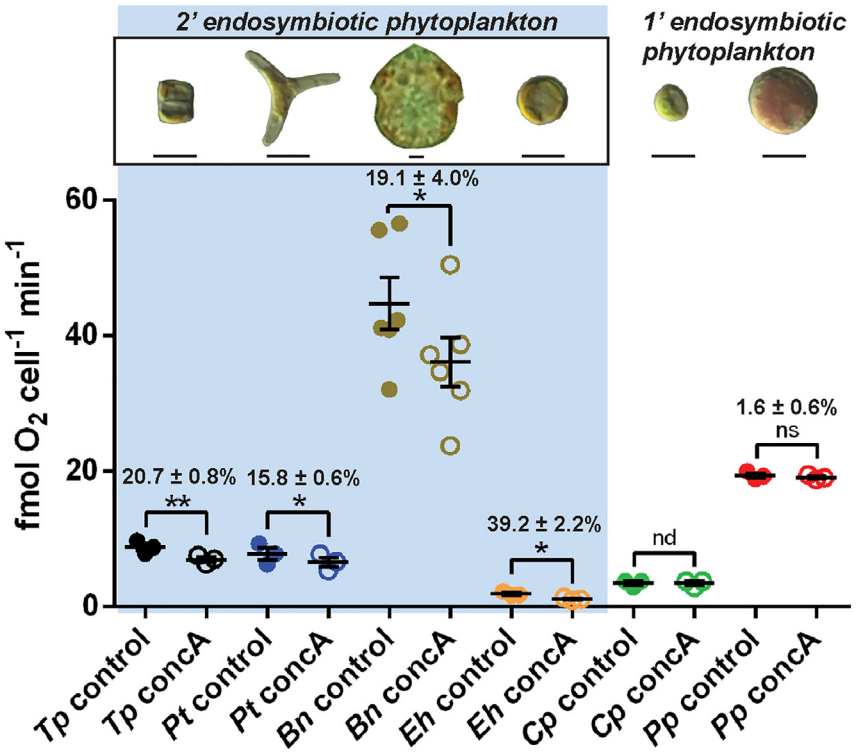

Figure 1. VHA contribution to O_2 production by marine microalgae

Gross O_2 production in control (vehicle DMSO; closed circles) and VHA-inhibited (concA = 10 nM concanamycin A; open circles) cultures. Percent reduction of O_2 production between control and VHA-inhibited cultures and p values are displayed above dot plots.

Tp, *T. pseudonana* (centric diatom); *Pt*, *P. tricornutum* (pennate diatom); *Bn*, *Brandtodinium nutricula* (dinoflagellate); *Eh*, *E. huxleyi* (coccolithophore); *Cp*, *C. prototheocoides* (green microalgae); *Pp*, *P. purpureum* (red microalgae).

Error bars, SEM; n = 3 except *Bn* (n = 6); paired t test: * $p < 0.05$; ** $p < 0.01$; nd, no difference; ns, no significant difference; scale bars: 5 μm.

See also Figure S1 and Table S1.

Transcriptomic analysis of synchronized cultures of *T. pseudonana* demonstrated constitutive mRNA expression of all VHA subunits, suggesting that VHA is important throughout the cell cycle (Figure 2B). However, the VHA holoenzyme can have multiple subcellular localizations and functions.[19,20] In diatoms, VHA has been reported in the membranes of vacuoles,[21] chloroplast endoplasmic reticulum[22] (cER), and silica deposition vesicles (SDVs), where it is strictly required for biomineralization of the silica cell wall and cell division.[21,23] The complexity and functional versatility of VHA are challenges for genetic manipulation approaches that would constitutively destabilize multiple physiological functions and confound phenotypic interpretation. They also rule out the use of transcriptomics to infer the physiological role(s) of VHA, as these analyses cannot not provide information about the subcellular localization of the VHA holoenzyme.

To better elucidate the mechanism by which VHA stimulates photosynthesis, we first explored whether concanamycin A affected variable chlorophyll a fluorescence yield. However, the maximum quantum yield of photosynthesis (F_v/F_m) and electron transport rate (ETR_{PSII}) were unaffected in VHA-inhibited cells (Figures S2A and S2B), indicating that VHA acts independently of photosynthetic light harvesting. Second, we wanted to ensure that decreased O_2 production with concanamycin A was not due to the inhibition of the known role of VHA in silica cell wall biomineralization.[21] In silicon-starved *T. pseudonana* where frustule formation is halted, we found that concanamycin A still significantly inhibited O_2 production (Figure S2C), proving that VHA is independently involved in both cell wall synthesis and photosynthesis.

Decades ago, it was proposed that VHA played role in transporting DIC for photosynthesis in secondary endosymbiotic phytoplankton.[4,5] If this is true, then providing a source of additional CO_2 should alleviate the effect of VHA inhibition on photosynthesis. Indeed, bubbling cells with 2% CO_2 rescued O_2 production by *T. pseudonana* treated with concanamycin A, while having no effect on controls (Figure S2D). We further sought to confirm that, in addition to O_2 production, VHA contributed to carbon fixation and incorporation into individual *T. pseudonana* cells. Using nanoscale secondary ion mass spectrometry (NanoSIMS) after incubation with ^{13}C-labeled DIC enabled us to obtain isotope incorporation data at the single-cell level (Figure S2E) and revealed that VHA inhibition induced a ~58% decrease in net photosynthetic biomass accretion (Figure S2F). Additionally, we could observe that carbon fixation was heterogeneous among cells, likely reflecting individual responses to different microscale gradients and/or metabolic feedbacks.[24]

A comparable stimulatory effect of VHA on photosynthetic O_2 production has recently been reported for photosymbiotic coral,[6] anemone,[8] and giant clam.[7] In all cases, VHA is present in host cellular membranes that interface with symbiotic algae, and VHA-dependent acidification of the microenvironment surrounding the algae contributes to a carbon-concentrating mechanism (CCM).[6] Thus, we hypothesized that VHA would be present in intracellular membranes of endosymbiotic origin surrounding the chloroplast. To establish the subcellular localization of VHA in diatoms, we performed microscopy on live transgenic *T. pseudonana* expressing EGFP-tagged VHA subunit B.[21] Airyscan confocal microscopy allowed us to create 3D reconstructions that revealed the presence of VHA around chloroplasts consistent with the cER or periplastid (PP) membranes (Figure 2C). This VHA localization was present throughout the cell cycle, and in dividing cells, it co-occurred with previously described localization in SDVs. Although Airyscan confocal microscopy can provide 140 nm lateral resolution (sometimes referred to as "super-resolution"),[25] the distance between the cER and PP membranes is tens of nanometers[26,27] apart; therefore, we were

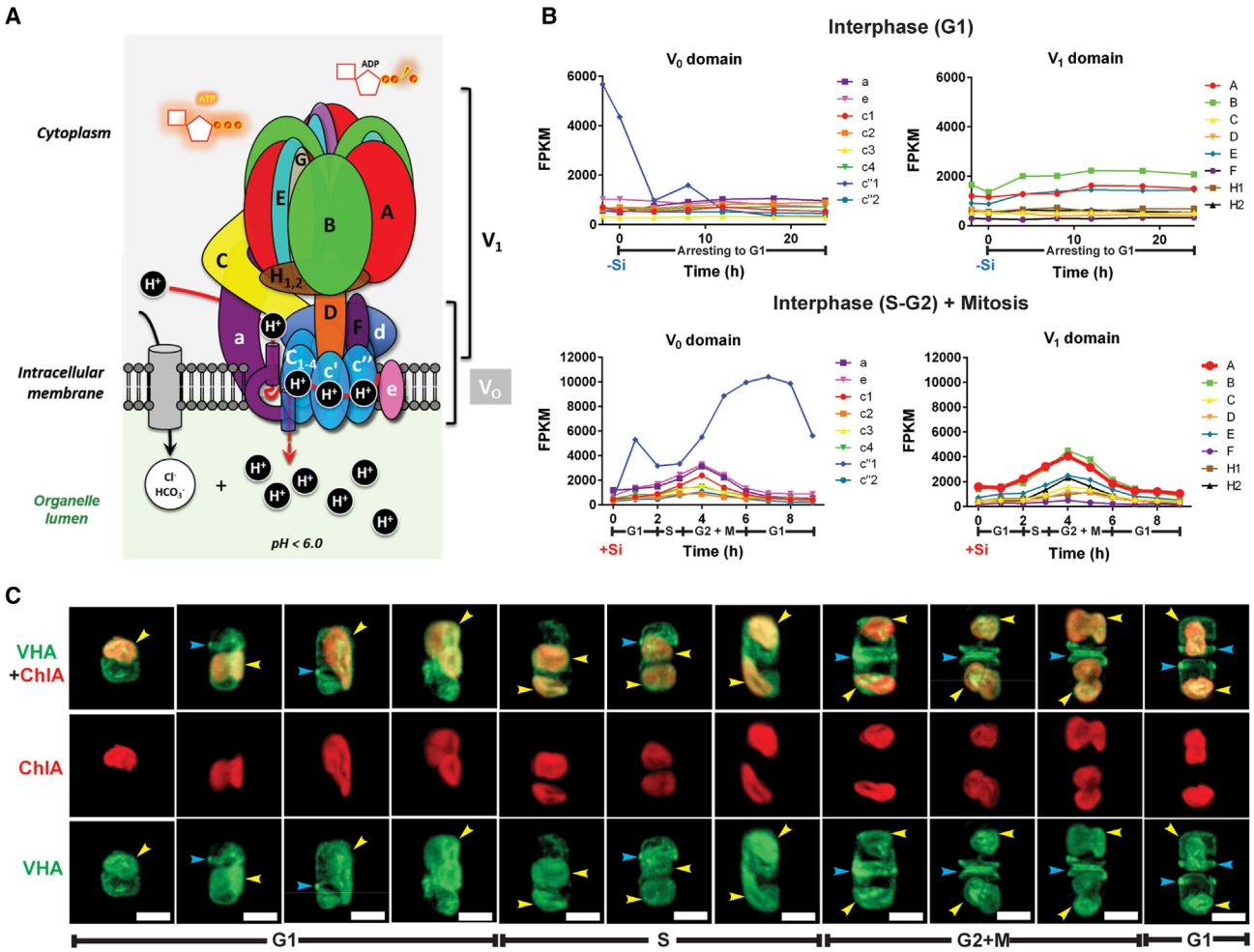

Figure 2. Expression and subcellular localization of VHA in *T. pseudonana*

(A) Diagram of the VHA-holoenzyme complex.

(B) Transcriptomic profile of VHA subunits during G1 (cell-cycle arrest following silicon starvation; top), and G1-S-G2+mitosis (synchronous division following silicon re-addition; bottom).

(C) 3D confocal images of EGFP-tagged VHA_B around chloroplasts (yellow arrows) and silica deposition vesicles (blue arrows) at different cell-cycle stages; scale bars: 5 μm.

See also Figures S2 and S3.

unable to determine the precise localization of VHA in one or both of these membranes. The small space between diatom chloroplast membranes also precluded measurements using pH-sensing dyes because the signal overwhelmingly accumulated in the thylakoid lumen, which is acidified during photosynthesis. In the future, this could possibly be overcome using genetically encoded ratiometric pH-sensitive sensors[28] targeted to the cER/PP membranes and oriented toward the external chloroplast microenvironment.

Nevertheless, VHA is a universal feature of eukaryotic cells and is present in a number of organelles, including endosomes, phagosomes, macropinosomes, lysosomes, Golgi, and melanosomes.[12] Since VHA invariably acidifies the lumen of each of these organelles to pH $\leq$ 6, we deduce that VHA in the cER/PP membranes of *T. pseudonana* must accomplish a similar effect. This is significant, because at pH $\leq$ 6.3, the majority of DIC equilibrates to CO_2.[29] Hence, we propose that VHA promotes CO_2 accumulation in the microenvironment external to the chloroplast. Consistent with model simulations of DIC fluxes in the diatom CCM,[30] some of the CO_2 would diffuse back into the cytoplasm (pH $\sim$ 7.2). However, the higher pH in the chloroplast stroma (pH $\sim$ 8.15) establishes a more favorable partial pressure gradient for CO_2 diffusion into this compartment (Figure S3B). The next steps follow the established CCM of microalgae.[31,32] In the stroma, CO_2 is immediately hydrated into HCO_3^- under catalysis by carbonic anhydrase, which is shuttled into the thylakoid lumen where pH is $\leq$ 6 due to H^+ pumping associated with photosynthetic electron transport chain. At the acidic pH, HCO_3^- dehydrates into CO_2 and diffuses into the pyrenoid matrix, saturating RuBisCo to maximize carbon fixation rates.

Altogether, our evidence supports the nearly 25-year-old hypothesis that the additional intracellular membranes of secondary endosymbiotic phytoplankton are derived from the ancestral "food vacuole" that engulfed red algae and contain "proton

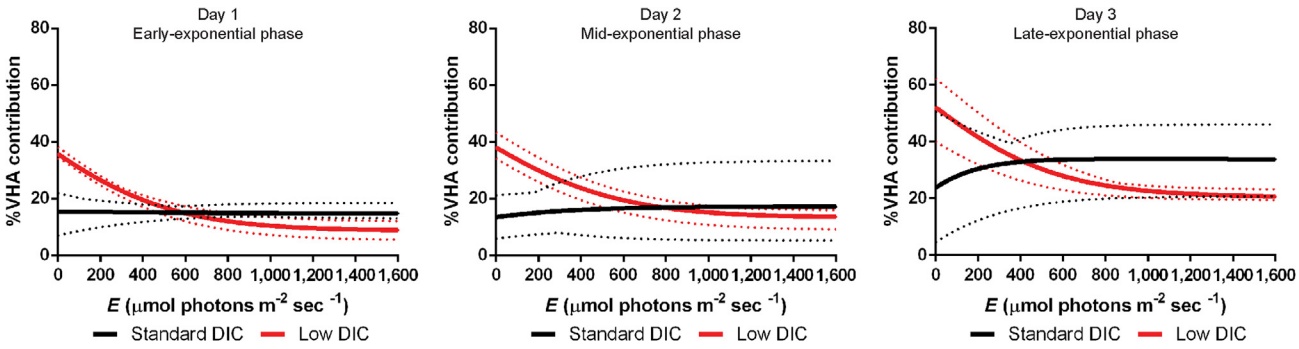

Figure 3. VHA contribution to carbon fixation in *T. pseudonana*

Contribution of VHA to bulk ^{14}C incorporation over the full range of oceanic irradiances, at three stages of growth, and at standard (1.92 mM; black lines; n = 6) and low (1.60 mM; red lines; n = 3) seawater DIC levels (dotted lines = 95% CI).

See also Figure S4 and Tables S2 and S3.

pumps" that contribute to a CCM around the chloroplast to enhance photosynthesis.[4,5] That hypothesis also predicted that secondary endosymbiotic phytoplankton must actively take up HCO_3^- from the environment, which has subsequently been confirmed in diatoms through the molecular and functional identification of SLC4 transporters in the plasmalemma.[33,34] However, the ionic and pH regulatory mechanisms that drive HCO_3^- transport across the various intracellular membranes of secondary endosymbiotic chloroplasts has remained elusive.[31] Our results indicate that VHA activity is one of such mechanisms, although not necessarily the only one.

Ecophysiological significance of the VHA-mediated diatom CCM

Lastly, we wanted to assess the significance of VHA-mediated carbon fixation by *T. pseudonana* in various physiological states and in response to a range of environmentally relevant levels of light and DIC. This was accomplished by generating photosynthesis versus irradiance (P-E) curves using the traditional and highly sensitive radioactive ^{14}C isotope incorporation method[35] over 1 h incubations. To capture the different physiological stages of cells during a bloom,[36] measurements were taken during early-, mid-, and late-exponential growth phases over 3 days of culturing. To assess the broad range of oceanic irradiances resulting from latitude, clouding, depth, and ocean mixing,[37] P-E curves were measured and fitted from 0 to 1,600 μmol photons m^{-2} s^{-1}. Lastly, to examine the response to rapid environmental DIC changes, incubations were conducted at ~2.0 mM (standard) and ~1.6 mM (low) environmental DIC-encompassing levels in the open ocean and coastal environments affected by rainfall, ice melting, and terrestrial freshwater inputs[38–40] (Figure S4; Table S2).

In these experiments, VHA inhibition impaired carbon fixation by at least 13.5% and as much as 52%. Under standard DIC, the contribution of VHA to carbon fixation was relatively constant across irradiances and rose from ~15% on day 1% to ~30% on day 3 (Figure 3; black curves). This trend suggests that *T. pseudonana* relies on VHA for maintaining photosynthetic rates as competition for DIC increases with cell density. In assays carried out under low DIC, the contribution of VHA to carbon fixation also rose from day 1 to 3; however, it gained additional importance at irradiances under 500 μmol photons m^{-2} s^{-1}. Strikingly, at sub-saturating irradiances of <100 μmol photons m^{-2} s^{-1}, the contribution of VHA to carbon fixation approached 40% on days 1–2 and surpassed 50% on day 3 of culturing (Figure 3; red curves). Because the bulk of phytoplankton productivity in the ocean occurs at the deep chlorophyll maximum (25–200 m depth) where irradiance is severely attenuated,[41,42] our results imply that VHA-mediated photosynthesis is most relevant in diatom-dominated phytoplankton assemblages where competition for DIC is high and light is limiting.

In summary, O_2 production, ^{13}C-NanoSIMS, and ^{14}C-P-E measurements demonstrated that VHA significantly contributes to photosynthetic carbon fixation that is retained as biomass. Given that diatoms contribute nearly 50% of carbon fixation in the ocean,[43,44] the component of photosynthesis that depends on VHA represents between ~7% and 25% of oceanic primary production, or between 3.5 and 13.5 Gtons of fixed carbon per year (Table S3). These numbers can only increase after accounting for VHA-mediated photosynthesis in other secondary endosymbiotic phytoplankton (Figure 1) and photosymbiotic invertebrates.[6–8] In addition, diatoms constitute about half of the biomass that sinks into the ocean's interior.[1,45] Based on our measurements of the contribution of VHA on both gross and net productivity in diatoms, VHA-mediated carbon fixation is poised to significantly contribute to the biological pump that shuttles organic carbon to the ocean's interior and, on a geologic time scale, to the biomass buried in the continental margin that formed fossil fuel deposits.[46] Even by the most conservative estimate, the cooption of VHA for the enhancement of photosynthesis is a symbiosis-derived evolutionary innovation with global environmental implications.

Perspectives on VHA-enhanced photosynthesis across marine photosymbioses

Engulfment of food particles by phagocytosis followed by lysosomal digestion is ubiquitously used by eukaryotic cells,[3] protists,[47] and invertebrate animals.[48] Acidification by VHA, which is conserved in all eukaryotes, is essential to these processes.[20] The presence of VHA in the cER/PP membranes that surround the chloroplasts of diatoms, as well as in the symbiosome membrane that surrounds the endosymbiotic microalgae of coral[6] and anemones,[8] establishes clear structural and enzymatic links between phagocytosis, endosymbiosis, and symbiogenesis

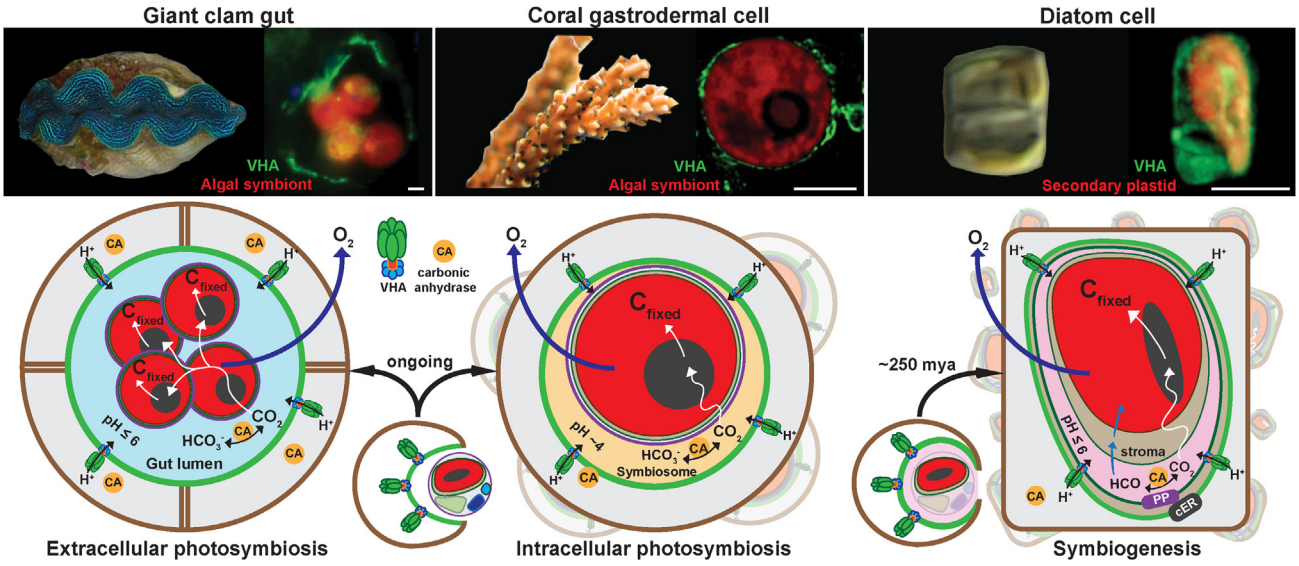

Figure 4. VHA-enhanced photosynthesis across marine photosymbioses

VHA in the photosymbiotic membrane interface promotes photosynthesis at multiple stages of photosymbiotic integration: (1) the apical membrane of epithelial cells of giant clam gut tubules hosting microalgae,[7] (2) the symbiosomal membrane of coral gastrodermal cells hosting microalgae,[6] and (3) the additional intracellular membranes (cER, chloroplast endoplasmic reticulum; PP, periplastid) of phagocytic origin that surround the chloroplasts of secondary endosymbiotic phytoplankton. Once CO_2 enters symbiotic algae and chloroplast, it follows canonical CCM mechanisms toward the site of RuBisCo; for simplicity, these steps are not depicted. Scale bars: 5 μm.

(Figure 4). The symbiotic microalgae of giant clams are hosted in the gut lumen and are therefore extracellular; however, they are surrounded by the apical membrane of the gut epithelium, which is also host-derived, contains VHA, and serves for food digestion.[7] Interestingly, all of these organisms rely on carbonic anhydrases to transport DIC to serve as substrate for photosynthesis,[49–51] and these enzymes tend to be functionally coupled with VHA to acidify intra- and extracellular compartments for diverse functions,[19] including lysosomal[52] and epithelial digestion.[53] Moreover, active acidification of a compartment will invariably displace the DIC equilibrium toward CO_2.[29] Therefore, enhancement of photosynthesis by VHA is consistent with fundamental principles of acid-base chemistry and cell biology.

The conserved role of VHA in enhancing photosynthesis in diverse marine photosymbioses is an exciting case of convergent evolution at the molecular level. Given the ubiquity of VHA-driven phagocytosis, we would expect to find analogous VHA-CCMs in other photosymbiotic protists and invertebrates. However, integration of host and endosymbiont into a single organism additionally requires significant gene remodeling and machinery to target and import proteins to the emerging organelle, which are very complex processes, and it is therefore a major constraint for symbiogenesis.[47] Nevertheless, the co-option of VHA from intracellular digestion to photosynthetic enhancement confers obvious advantages to extant secondary endosymbiotic marine phytoplankton, particularly in competitive DIC- and light-limited environments, which, in turn, has lasting impacts on ocean carbon biogeochemical cycles. Since this advantage is also evident in extant photosymbiotic invertebrates, we speculate it similarly applied to the ancestral heterotrophic protist(s) that engulfed red microalgae during the transitional stages throughout endosymbiosis and symbiogenesis. Therefore, VHA-enhancement of photosynthesis would have provided both a trait for positive selection and an evolutionary advantage over other phytoplankton in the low-CO_2 Permian oceans where secondary endosymbiotic phytoplankton began their diversification and ecological dominance.[4,5]

STAR★METHODS

Detailed methods are provided in the online version of this paper and include the following:

- KEY RESOUCES TABLE
- RESOURCE AVAILABILITY
  - Lead contact
  - Materials availability
  - Data and code availability
- EXPERIMENTAL MODEL AND SUBJECT DETAILS
- METHOD DETAILS
  - Culture and growth data
  - Transcriptomics
  - 3D Confocal Microscopy
  - Oxygen measurements
  - Pulse amplitude modulated fluorometry
  - Nanoscale secondary ion mass spectrometry
  - ^{14}C photosynthesis versus irradiance curves
  - P-E curve fitting and calculation of VHA contribution
- QUANTIFICATION AND STATISTICAL ANALYSIS

SUPPLEMENTAL INFORMATION

Supplemental information can be found online at https://doi.org/10.1016/j.cub.2023.05.020.

ACKNOWLEDGMENTS

We are grateful for the help of Dr. Roshan Shrestha who provided plasmids and assistance with cloning and transformations; Dr. Brian Palenik and Dr. Giovanni Finazzi who provided oxygen measurement equipment; and Dr. Orna Cook and Dr. Charlotte LeKieffre who provided microalgae cultures. Dr. Christopher Hewes assisted with fluorometric chlorophyll measurements. Dr. Garfield Kwan, Angus Thies, and Dr. Eric Armstrong provided images for Figure 4. Four reviewers and the journal editor provided valuable comments that helped improve the manuscript. Work carried out by D.P.Y. was partially supported by the National Institutes of Health Training Program in Marine Biotechnology grant T32-GM067550, the IDEX project of the University of Grenoble Alpes, and the European Molecular Biology Laboratory. The Arthur M. and Kate E. Tode Research Endowment in Marine Biological Sciences (UCSD) provided M.T. with essential equipment used in this project. Work at LLNL was performed under the auspices of US Department of Energy Office of Science contract DE-AC52-07NA27344.

AUTHOR CONTRIBUTIONS

Conceptualization, M.T. and D.P.Y.; methodology, D.P.Y., M.T., M.H., T.J.S., X.M., P.K.W., M.V., and B.G.M.; formal analysis, D.P.Y., M.T., R.M.A., T.J.S., X.M., and P.K.W.; investigation, D.P.Y., B.S., R.M.A., T.J.S., and M.T.; resources, M.T., X.M., M.V., B.G.M., M.H., and J.D.; writing – original draft, D.P.Y. and M.T.; writing – review & editing, D.P.Y., M.T., T.J.S., X.M., P.K.W., R.M.A., M.V., B.G.M., and J.D.; funding acquisition, M.T., D.P.Y., T.J.S., X.M., and P.K.W.

DECLARATION OF INTERESTS

The authors declare no competing interests.

Received: September 19, 2022
Revised: March 20, 2023
Accepted: May 9, 2023
Published: May 31, 2023

REFERENCES

1. Falkowski, P.G., Katz, M.E., Knoll, A.H., Quigg, A., Raven, J.A., Schofield, O., and Taylor, F.J. (2004). The evolution of modern eukaryotic phytoplankton. Science *305*, 354–360.
2. Keeling, P.J. (2010). The endosymbiotic origin, diversification and fate of plastids. Philos. Trans. R. Soc. Lond. B Biol. Sci. *365*, 729–748.
3. Saftig, P., and Klumperman, J. (2009). Lysosome biogenesis and lysosomal membrane proteins: trafficking meets function. Nat. Rev. Mol. Cell Biol. *10*, 623–635.
4. Lee, R.E., and Kugrens, P. (2000). Ancient atmospheric CO2 and the timing of evolution of secondary endosymbioses. Phycologia *39*, 167–172.
5. Lee Edward, R., and Kugrens, P. (1998). Hypothesis: the ecological advantage of chloroplast ER – the ability to outcompete at low dissolved CO2 concentrations. Protist *149*, 341–345.
6. Barott, K.L., Venn, A.A., Perez, S.O., Tambutté, S., and Tresguerres, M. (2015). Coral host cells acidify symbiotic algal microenvironment to promote photosynthesis. Proc. Natl. Acad. Sci. USA *112*, 607–612.
7. Armstrong, E.J., Roa, J.N., Stillman, J.H., and Tresguerres, M. (2018). Symbiont photosynthesis in giant clams is promoted by V-type H+-ATPase from host cells. J. Exp. Biol. *221*, 1–7.
8. Barott, K.L., Thies, A.B., and Tresguerres, M. (2022). V-type H + -ATPase in the symbiosome membrane is a conserved mechanism for host control of photosynthesis in anthozoan photosymbioses. R. Soc. Open Sci. *9*, 211449.
9. Dröse, S., and Altendorf, K. (1997). Bafilomycins and concanamycins as inhibitors of V-ATPases and P-ATPases. J. Exp. Biol. *200*, 1–8.
10. Dröse, S., Bindseil, K.U., Bowman, E.J., Siebers, A., Zeeck, A., and Altendorf, K. (1993). Inhibitory effect of modified bafilomycins and concanamycins on P- and V-type adenosinetriphosphatases. Biochemistry *32*, 3902–3906.
11. Kriegel, A., Andrés, Z., Medzihradszky, A., Krüger, F., Scholl, S., Delang, S., Patir-Nebioglu, M.G., Gute, G., Yang, H., Murphy, A.S., et al. (2015). Job sharing in the endomembrane system: vacuolar acidification requires the combined activity of V-ATPase and V-PPase. Plant Cell *27*, 3383–3396.
12. Freeman, S.A., Grinstein, S., and Orlowski, J. (2023). Determinants, maintenance, and function of organellar pH. Physiol. Rev. *103*, 515–606.
13. Bowman, B.J., and Bowman, E.J. (2002). Mutations in subunit c of the vacuolar ATPase confer resistance to bafilomycin and identify a conserved antibiotic binding site. J. Biol. Chem. *277*, 3965–3972.
14. Bowman, E.J., Graham, L.A., Stevens, T.H., and Bowman, B.J. (2004). The bafilomycin/concanamycin binding site in subunit c of the V-ATPases from *Neurospora crassa* and *Saccharomyces cerevisiae*. J. Biol. Chem. *279*, 33131–33138.
15. Bhattacharya, D., Price, D.C., Xin Chan, C., Qiu, H., Rose, N., Ball, S., Weber, A.P.M., Cecilia Arias, M., Henrissat, B., Coutinho, P.M., et al. (2013). Genome of the red alga *Porphyridium purpureum*. Nat. Commun. *4*, 1–10.
16. Yagisawa, F., Nishida, K., Yoshida, M., Ohnuma, M., Shimada, T., Fujiwara, T., Yoshida, Y., Misumi, O., Kuroiwa, H., and Kuroiwa, T. (2009). Identification of novel proteins in isolated polyphosphate vacuoles in the primitive red alga *Cyanidioschyzon merolae*. Plant J. *60*, 882–893.
17. Li, J., Pan, K., Tang, X., Li, Y., Zhu, B., and Zhao, Y. (2021). The molecular mechanisms of *Chlorella* sp. responding to high CO2: a study based on comparative transcriptome analysis between strains with high- and low-CO_2 tolerance. Sci. Total Environ. *763*, 1–9.
18. Hildebrand, M., Frigeri, L.G., and Davis, A.K. (2007). Synchronized growth of *Thalassiosira pseudonana* (Bacillariophyceae) provides novel insights into cell-wall synthesis processes in relation to the cell cycle 1. J. Phycol. *43*, 730–740.
19. Tresguerres, M. (2016). Novel and potential physiological roles of vacuolar-type H+-ATPase in marine organisms. J. Exp. Biol. *219*, 2088–2097.
20. Nishi, T., and Forgac, M. (2002). The vacuolar (H^+)-ATPases — nature's most versatile proton pumps. Nat. Rev. Mol. Cell Biol. *3*, 94–103.
21. Yee, D.P., Hildebrand, M., and Tresguerres, M. (2020). Dynamic subcellular translocation of V-type H+ -ATPase is essential for biomineralization of the diatom silica cell wall. New Phytol. *225*, 2411–2422.
22. Bussard, A., and Lopez, P.J. (2014). Evolution of vacuolar pyrophosphatases and vacuolar H^+-ATPases in diatoms. J. Mar. Sci. Technol. *22*, 50–59.
23. Vartanian, M., Desclés, J., Quinet, M., Douady, S., and Lopez, P.J. (2009). Plasticity and robustness of pattern formation in the model diatom *Phaeodactylum tricornutum*. New Phytol. *182*, 429–442.
24. Samo, T.J., Kimbrel, J.A., Nilson, D.J., Pett-Ridge, J., Weber, P.K., and Mayali, X. (2018). Attachment between heterotrophic bacteria and microalgae influences symbiotic microscale interactions. Environ. Microbiol. *20*, 4385–4400.
25. Huff, J. (2015). The Airyscan detector from ZEISS: confocal imaging with improved signal-to-noise ratio and super-resolution. Nat. Methods *12*. i–ii.
26. Flori, S., Jouneau, P.H., Finazzi, G., Maréchal, E., and Falconet, D. (2016). Ultrastructure of the periplastidial compartment of the diatom *Phaeodactylum tricornutum*. Protist *167*, 254–267.
27. Bedoshvili, Y.D., Popkova, T.P., and Likhoshway, Y.V. (2009). Chloroplast structure of diatoms of different classes. Cell Tissue Biol. *3*, 297–310.
28. Karsten, L., Goett-Zink, L., Schmitz, J., Hoffrogge, R., Grünberger, A., Kottke, T., and Müller, K.M. (2022). Genetically encoded ratiometric pH sensors for the measurement of intra-and extracellular pH and internalization rates. Biosensors *12*, 271.
29. Tresguerres, M., Clifford, A.M., Harter, T.S., Roa, J.N., Thies, A.B., Yee, D.P., and Brauner, C.J. (2020). Evolutionary links between intra- and extracellular acid–base regulation in fish and other aquatic animals. J. Exp. Zool. A Ecol. Integr. Physiol. *333*, 449–465.

30. Hopkinson, B.M., Dupont, C.L., Allen, A.E., and Morel, F.M.M. (2011). Efficiency of the CO2-concentrating mechanism of diatoms. Proc. Natl. Acad. Sci. USA *108*, 3830–3837.
31. Matsuda, Y., Hopkinson, B.M., Nakajima, K., Dupont, C.L., and Tsuji, Y. (2017). Mechanisms of carbon dioxide acquisition and CO2 sensing in marine diatoms: A gateway to carbon metabolism. Philos. Trans. R. Soc. Lond. B Biol. Sci. *372*, 1–12.
32. Fei, C., Wilson, A.T., Mangan, N.M., Wingreen, N.S., and Jonikas, M.C. (2022). Modelling the pyrenoid-based CO2-concentrating mechanism provides insights into its operating principles and a roadmap for its engineering into crops. Nat. Plants *8*, 583–595.
33. Nakajima, K., Tanaka, A., and Matsuda, Y. (2013). SLC4 family transporters in a marine diatom directly pump bicarbonate from seawater. Proc. Natl. Acad. Sci. USA *110*, 1767–1772.
34. Nawaly, H., Matsui, H., Tsuji, Y., Iwayama, K., Ohashi, H., Nakajima, K., and Matsuda, Y. (2023). Multiple plasma membrane SLC4s contribute to external HCO3– acquisition during CO2 starvation in the marine diatom *Phaeodactylum tricornutum*. J. Exp. Bot. *74*, 296–307.
35. Nielsen, E.S. (1952). The use of radio-active carbon (c14) for measuring organic production in the sea. ICES J. Mar. Sci. *18*, 117–140.
36. Saito, H., and Tsuda, A. (2003). Influence of light intensity on diatom physiology and nutrient dynamics in the Oyashio region. Prog. Oceanogr. *57*, 251–263.
37. Hoffmann, L.J., Peeken, I., and Lochte, K. (2008). Iron, silicate, and light co-limitation of three Southern Ocean diatom species. Polar Biol. *31*, 1067–1080.
38. Smetacek, V., Klaas, C., Strass, V.H., Assmy, P., Montresor, M., Cisewski, B., Savoye, N., Webb, A., D'Ovidio, F., Arrieta, J.M., et al. (2012). Deep carbon export from a Southern Ocean iron-fertilized diatom bloom. Nature *487*, 313–319.
39. Wang, Z.A., Wanninkhof, R., Cai, W.J., Byrne, R.H., Hu, X., Peng, T.H., and Huang, W.J. (2013). The marine inorganic carbon system along the Gulf of Mexico and Atlantic coasts of the United States: insights from a transregional coastal carbon study. Limnol. Oceanogr. *58*, 325–342.
40. Liu, Q., Charette, M.A., Henderson, P.B., McCorkle, D.C., Martin, W., and Dai, M. (2014). Effect of submarine groundwater discharge on the coastal ocean inorganic carbon cycle. Limnol. Oceanogr. *59*, 1529–1554.
41. Valenti, D., Denaro, G., Spagnolo, B., Conversano, F., and Brunet, C. (2015). How diffusivity, thermocline and incident light intensity modulate the dynamics of deep chlorophyll maximum in Tyrrhenian sea. PLoS One *10*, e0115468.
42. Mignot, A., Claustre, H., Uitz, J., Poteau, A., D'Ortenzio, F., and Xing, X. (2014). Understanding the seasonal dynamics of phytoplankton biomass and the deep chlorophyll maximum in oligotrophic environments: a Bio-Argo float investigation. Global Biogeochem. Cycles *28*, 856–876.
43. Field, C.B., Behrenfeld, M.J., Randerson, J.T., and Falkowski, P. (1998). Primary production of the biosphere: integrating terrestrial and oceanic components. Science *281*, 237–240.
44. Nelson, D.M., Tréguer, P., Brzezinski, M.A., Leynaert, A., and Quéguiner, B. (1995). Production and dissolution of biogenic silica in the ocean: revised global estimates, comparison with regional data and relationship to biogenic sedimentation. Global Biogeochem. Cycles *9*, 359–372.
45. Benoiston, A.S., Ibarbalz, F.M., Bittner, L., Guidi, L., Jahn, O., Dutkiewicz, S., and Bowler, C. (2017). The evolution of diatoms and their biogeochemical functions. Philos. Trans. R. Soc. Lond. B Biol. Sci. *372*, 1–10.
46. Falkowski, P.G., Katz, M.E., Milligan, A.J., Fennel, K., Cramer, B.S., Aubry, M.P., Berner, R.A., Novacek, M.J., and Zapol, W.M. (2005). The rise of oxygen over the past 205 million years and the evolution of large placental mammals. Science *309*, 2202–2204.
47. Cavalier-Smith, T. (2013). Symbiogenesis: mechanisms, evolutionary consequences, and systematic implications. Ann. Rev. Ecol. Evol. Syst. *44*, 145–172.
48. He, C., Han, T., Liao, X., Zhou, Y., Wang, X., Guan, R., Tian, T., Li, Y., Bi, C., Lu, N., et al. (2018). Phagocytic intracellular digestion in amphioxus (*Branchiostoma*). Proc. Biol. Sci. *285*, 1–10.
49. Reinfelder, J.R. (2011). Carbon concentrating mechanisms in eukaryotic marine phytoplankton. Ann. Rev. Mar. Sci. *3*, 291–315.
50. Bertucci, A., Moya, A., Tambutté, S., Allemand, D., Supuran, C.T., and Zoccola, D. (2013). Carbonic anhydrases in anthozoan corals – a review. Bioorg. Med. Chem. *21*, 1437–1450.
51. Yellowlees, D., Dionisio-Sese, M.L., Masuda, K., Maruyama, T., Abe, T., Baillie, B., Tsuzuki, M., and Miyachi, S. (1993). Role of carbonic anhydrase in the supply of inorganic carbon to the giant clam-zooxanthellate symbiosis. Mar. Biol. *115*, 605–611.
52. Caricato, R., Giordano, M.E., Schettino, T., and Lionetto, M.G. (2018). Functional involvement of carbonic anhydrase in the lysosomal response to cadmium exposure in *Mytilus galloprovincialis* digestive gland. Front. Physiol. *9*, 319.
53. Andrikou, C., Thiel, D., Ruiz-Santiesteban, J.A., and Hejnol, A. (2019). Active mode of excretion across digestive tissues predates the origin of excretory organs. PLoS Biol. *17*, e3000408.
54. Smith, S.R., Glé, C., Abbriano, R.M., Traller, J.C., Davis, A., Trentacoste, E., Vernet, M., Allen, A.E., and Hildebrand, M. (2016). Transcript level coordination of carbon pathways during silicon starvation-induced lipid accumulation in the diatom *Thalassiosira pseudonana*. New Phytol. *210*, 890–904.
55. Silsbe, G., and Malkin, S. (2015). Phytotools: phytoplankton production tools. R package version 1.0. https://CRAN.R-project.org/package=phytotools.
56. Lewis, E., and Wallace, D. (1998). Program developed for CO2 system calculations. ORNL Cdiac *105*, 1–21.
57. Holm-Hansen, O., Lorenzen, C.J., Holmes, R.W., and Strickland, J.D.H. (1965). Fluorometric determination of chlorophyll. ICES J. Mar. Sci. *30*, 3–15.
58. Ritchie, R.J. (2006). Consistent sets of spectrophotometric chlorophyll equations for acetone, methanol and ethanol solvents. Photosynth. Res. *89*, 27–41.
59. Edgar, R., Domrachev, M., and Lash, A.E. (2002). Gene expression omnibus: NCBI gene expression and hybridization array data repository. Nucleic Acids Res. *30*, 207–210.
60. Wei, L., Shen, C., El Hajjami, M., You, W., Wang, Q., Zhang, P., Ji, Y., Hu, H., Hu, Q., Poetsch, A., et al. (2019). Knockdown of carbonate anhydrase elevates *Nannochloropsis* productivity at high CO2 level. Metab. Eng. *54*, 96–108.
61. Martin, C.L., and Tortell, P.D. (2008). Bicarbonate transport and extracellular carbonic anhydrase in marine diatoms. Physiol. Plant. *133*, 106–116.
62. Darley, W.M., and Volcani, B.E. (1969). Role of silicon in diatom metabolism: a silicon requirement for deoxyribonucleic acid synthesis in the diatom *Cylindrotheca fusiformis* Reimann and Lewin. Exp. Cell Res. *58*, 334–342.
63. Pett-Ridge, J., and Weber, P.K. (2012). NanoSIP: NanoSIMS applications for microbial biology. In Methods in Molecular Biology, A. Navid, ed. (Humana Press), pp. 375–408.
64. Pett-Ridge, J., and Weber, P.K. (2022). NanoSIP: NanoSIMS applications for microbiology. In Microbial Systems Biology, A. Navid, ed. (Human Press Incorp.), pp. 91–136.
65. Lewis, M., and Smith, J. (1983). A small volume, short-incubation-time method for measurement of photosynthesis as a function of incident irradiance. Mar. Ecol. Prog. Ser. *13*, 99–102.
66. Platt, T., Gallegos, C.L., and Harrison, W.G. (1980). Photoinhibition of photosynthesis in natural assemblages of marine phytoplankton. J. Mar. Res. *38*, 687–701.

STAR★METHODS

KEY RESOUCES TABLE

REAGENT or RESOURCE	SOURCE	IDENTIFIER
Chemicals, peptides, and recombinant proteins		
Concanamycin A	Adipogen	Cat #BVT-0237-M001
14C-NaHCO3	MP Biomedicals	Cat #MP0117441H2
13C-NaHCO3	Sigma-Aldrich	Cat #372382
Deposited data		
RNASeq for silicon replenished *T. pseudonana*	This paper	NCBI's Gene Expression Omnibus. Ascesion ID: GSE203136 (https://www.ncbi.nlm.nih.gov/geo/query/acc.cgi?acc=GSE203136)
RNASeq for silicon starved *T. pseudonana*	Smith[54]	NCBI's Gene Expression Omnibus. Ascesion ID: GSE75460 (https://www.ncbi.nlm.nih.gov/geo/query/acc.cgi?acc=GSE75460)
Experimental models: Cell lines		
T. pseudonana cell line expressing Fcp-VHA_B-EGFP	Yee et al.[21]	Tp-Fcp-VHAB-EGFP
Experimental models: Organisms/strains		
Thalassiosira pseudonana	Provasoli-Guillard National Center for Culture of Marine Phytoplankton	CCMP 1335
Phaeodactylum tricornutum	Provasoli-Guillard National Center for Culture of Marine Phytoplankton	CCMP 632
Brandtodinium nutricula	Roscoff Culture Collection	RCC3387
Porphyridium purpurneum	Provasoli-Guillard National Center for Culture of Marine Phytoplankton	CCMP1947
Emiliania huxleyi	Provasoli-Guillard National Center for Culture of Marine Phytoplankton	CCMP1516
Chlorella protothecoides	UTEX Culture Collection of Algae	CCAP-211/7a
Oligonucleotides		
Tp-VHA-B Forward Gateway cloning primer	Yee et al.[21]	DY1-16: GGGGACAAGTTTGT ACAAAAAAGCAGGCTT AATGGCATCCCACGCA GACGAAC
Tp-VHA-B Reverse Gateway cloning primer	Yee et al.[21]	DY1-17: GGGGACCAC TTTGTACAAGAAAGCT GGGTTGTTCGATCCATC TGCCTTGTTCAT
Recombinant DNA		
Tp-Fcp-VHAB-EGFP BP	Yee et al.[21]	Tp-Fcp-VHAB-EGFP BP
Tp-Fcp-VHAB-EGFP LR	Yee et al.[21]	Tp-Fcp-VHAB-EGFP LR
Software and algorithms		
Zen Blue	Carl Zeiss Microscopy GmbH	N/A

(*Continued on next page*)

Continued

REAGENT or RESOURCE	SOURCE	IDENTIFIER
O2view	Hansatech Instruments	N/A
Presens Measurement Studio 2.0	PreSens Precision Sensing GmbH	N/A
WinControl-3	Heinz Walz GmbH	N/A
Prism 6	GraphPad	https://www.graphpad.com
L'Image	Limage	https://limagesoftware.net
RStudio	RStudio	https://www.rstudio.com
Phytotools R-package	Silsbe and Malkin[55]	https://cran.r-project.org/package=phytotools
CO2Sys_v2.1	Lewis and Wallace[56]	https://cdiac.ess-dive.lbl.gov/ftp/co2sys/

RESOURCE AVAILABILITY

Lead contact

Further information and requests for resources and reagents should be directed to and will be fulfilled by the lead contact, Daniel Yee (daniel.p.yee@gmail.com).

Materials availability

Plasmids used for and transformed *T. pseudonana* expressing EGFP-tagged VHA subunit B cell line in this study will be shared by the lead contact upon request.

Data and code availability

- RNA-seq data have been deposited at NCBI's Gene Expression Omnibus and are publicly available as of the date of publication. Accession numbers are listed in the key resources table. Microscopy data reported in this paper will be shared by the lead contact upon request.
- This study did not generate new code.
- Any additional information required to reanalyze the data reported in this paper is available from the lead contact upon request.

EXPERIMENTAL MODEL AND SUBJECT DETAILS

This study used the following marine microalgae cell lines which were verified by their culture collection source. *Thalassiosira pseudonana* Hasle et Heimdale clone 3H CCMP 1335 (Provasoli-Guillard National Center for Culture of Marine Phytoplankton, Bigelow Laboratory for Ocean Sciences). *Phaeodactylum tricornutum* strain CCMP 632 (synonymous with the genome-sequenced strain CCMP2561). *Brandtodinium nutricula* stain RCC 3387; isolated from Collodaria in Villefranche-sur-Mer. *Porphyridium purpurneum* strain CCMP1947. *Emiliania huxleyi* strain CCMP 1516. *Chlorella protothecoides* strain UTEX 25 (CCAP-211/7a).

Cultures of *T. pseudonana* (CCMP1335), *T. pseudonana* expressing EGFP-tagged VHA_B,[21] *P. tricornutum* (CCMP632), *E. huxleyi* (CCMP1516), *P. purpurneum* (CCMP1947), and *C. protothecoides* (CCAP-211/7a) were grown axenically in F/2 medium prepared with seawater from the Scripps Pier. Inoculum cultures were maintained in 50 ml volumes in 125 ml Erlenmeyer flasks on an orbital shaker under continuous illumination provided by cool-white fluorescent lamps at 70 μmol photons m^{-2} s^{-1} at 18°C. Inoculum grown to ~2x10^6 cells ml^{-1} were used to inoculate 1 l bioreactor tubes bubbled with air and under continuous illumination by cool-white fluorescent lamps at ~100 μmol photons m^{-2} s^{-1} at 18°C at a starting density of 1x10^5 cells ml^{-1}. Cultures of *B. nutricula* (RCC3387) were grown in T25 tissue culture flasks (Falcon) with 25 ml of K2 medium prepared with seawater collected from Villefranche-sur-mer Marine Station. Cultures were inoculated at 4x10^4 cells ml^{-1} maintained at 70 μmol photons m^{-2} s^{-1} at 20°C without bubbling or agitation.

METHOD DETAILS

Culture and growth data

Daily measurements of cell count, chlorophyll content, pH, and total CO_2 (TCO_2) were collected over the duration of all culturing experiments except for *B. nutricula* in which only cell counts and chlorophyll content was collected. These measurements were used to calculate cellular chlorophyll content, specific growth rates, and carbonate chemistry. Cells were counted with a Neubauer hemacytometer chamber on a Zeiss inverted light microscope. Chlorophyll was measured on a Turner fluorometer following overnight

extraction in 100% methanol at -20℃. Relative fluorescence units were recorded before and after the addition of two drops 0.1 N HCl and total chlorophyll was calculated by the method described in Holm-Hansen et al.[57] *B. nutricula* chlorophyll was measured using a Multiskan SkyHigh Microplate UV-Vis spectrophotometer (Thermo Scientific) following overnight extraction in 100% methanol at -20℃ and calculated by the method described by Ritchie.[58]

Culture pH was measured using an UltraBASIC pH meter (Denver Instruments) equipped with an Orion glass pH electrode (ThermoFisher Scientific) calibrated with NBS standard buffer. Total CO_2 was measured using a Corning 965 Carbon Dioxide Analyzer with technical duplicates taken between 10 mM $NaCO_3$ standard measurements. Carbonate chemistry in the cultures was calculated using CO2Sys_v2.1[56] by inputting salinity, temperature, pH and TCO_2.

Transcriptomics

Transcriptomic datasets and analyses were performed as described in Yee et al.[21] In brief, the VHA mRNA expression levels Fragments Per Kilobase Million (FPKM) was acquired from transcriptomics analysis of RNAseq data collected from time-course experiments at 7 timepoints throughout 24 hours of silicon starvation and at 9 timepoints over 9 hours following silicon replenishment from biological duplicates of synchronized *T. pseudonana* cultures. The data discussed in this publication have been deposited in the NCBI's Gene Expression Omnibus[59] and are accessible through GEO Series accession number GSE75460 and GSE203136.

3D Confocal Microscopy

T. pseudonana expressing VHA_B-EGFP were loaded in 35 mm poly-d-lysine coated glass bottom dish and imaged with a Zeiss LSM800/900 inverted confocal microscopes equipped with a Zeiss Plan-Apochromat 63× (1.4) Oil DIC M27 objective, and Zeiss Airyscan super-resolution detector. Z-stacks were acquired to monitor EGFP (Ex 488 nm with 0.3% laser power, Em 509 nm, and detection 490-535 nm) and chlorophyll (Ex 488 nm with 0.2% laser power, Em 667 nm, detection 450-700 nm) fluorescence. Z-stack acquisition at ~150 nm thickness intervals were used to generate 3D images and exported using the Zen Blue software package (Carl Zeiss Microscopy GmbH).

Oxygen measurements

Individual cultures of *T. pseudonana*, *P. tricornutum*, *E. huxleyi*, *C. protothecoides*, and *P. purpurneum* grown in F/2 were maintained in exponential growth in 1 l bioreactor tubes bubbled with air and under continuous illumination by cool-white fluorescent lamps at ~100 μmol photons m^{-2} s^{-1} at 18℃. Cultures were sampled over multiple days to obtain replicate measurements of oxygen production rates. Replicate cultures of *B. nutricula* grown in K2 were maintained in exponential growth in T25 tissue culture flasks under a 12h light-dark cycle illuminated by cool-white fluorescent lamps at ~70 μmol photons m^{-2} s^{-1} at 20℃ were used to obtain oxygen data. Similar culture procedures for culturing *B. nutricula* were used for *T. pseudonana* for obtaining oxygen data for 2% CO_2 bubbling experiments. For measurement on silicon starved cultures, *T. pseudonana* were grown to $1x10^6$ cells/ml in K2 then washed three times in silicon free ESAW (-Si) by centrifugation at 4,200x g for 10 minutes before being resuspended and incubated in ESAW overnight.

Samples were pre-incubated with vehicle DMSO (control) or 10 nM concanamycin A (a highly specific of VHA[9]; Cat #: BVT-0237-M001) for 10 mins before measurement. For cultures grown in F/2, 1 ml of sample was used to measure oxygen on a Hansatech Oxylab Clark-type electrode operated with O2view software (Hansatech Instruments) and illuminated at 1,000 μmol photons m^{-2} sec^{-1} with stirring in a water-jacketed chamber maintained at 18°C. For *B. nutricula*, 2 ml of sample was used to measure oxygen production with an optical oxygen sensor operated with Presens Measurement Studio 2.0 (PreSens Precision Sensing GmbH) and illuminated at 500 μmol photons m^{-2} sec^{-1} with stirring at room temperature (~20°C). For *T. pseudonana* CO_2 rescue experiments, sample was buffered with 50 mM HEPES pH 8.0 solution[60,61] prior to bubbling for 3 minutes with air balanced 2% CO_2 produced with a GMS150 gas mixing system (Photon Systems Instruments). For *T. pseudonana* CO_2 rescue and –Si experiments, 500 μl of sample was used to measure oxygen in a WALZ KS-2500 water-jacketed chamber (Heinz Walz GmbH) paired with a FSO2-1 oxygen meter and optical microsensor (PyroScience GmbH). Samples were illuminated at 625 μmol photons m^{-2} sec^{-1} with stirring at 20°C by a MINI-PAM-II controlled by WinControl-3 software (Heinz Walz GmbH).

Net maximum O_2 production was measured by calculating the slope of O_2 concentration over ~10 mins of illumination. Respiration was calculated similarly over 1 min immediately after illumination. Gross maximum production was calculated by the equation:

$$O_{2gross} = O_{2net} - \text{respiration}$$

O_2 production rates were analyzed in Graphpad Prism 6 (GraphPad Software, La Jolla California USA) by paired two-tailed t-test between control and concanamycin A treatments for each species. Oxygen production rates and P-values showing statistical significance between paired treatments are summarized in Table S1. The *T. pseudonana* CO_2 rescue experiments were analyzed by 2-way repeated measures ANOVA using "CO_2 level" (air or 2% CO2) and "Drug" (DMSO or concanamycin A) as factors, which yielded significant effects for the two factors and the interaction. The subsequent Šidàk's multiple comparison test revealed a significant effect of 2% CO_2 only in *T. pseudonana* treated with concanamycin A.

Pulse amplitude modulated fluorometry

Rapid light curves (30 second actinic light exposures; 300 ms saturating pulse) for electron transport rate through photosystem II were collected on triplicate cultures of *T. pseudonana* pre-incubated with vehicle DMSO (control) or 10 nM concanamycin A.

500 μl of sample was measured with stirring in a WALZ KS-2500 water-jacketed chamber maintained at 20°C by a Mini-PAM-II fluorometer operated with WinControl-3 software (Heinz Walz GmbH).

Nanoscale secondary ion mass spectrometry

T. pseudonana cells grown in F/2 were harvested from 1l tube bioreactors at ~1.6x10^6 cells/ml. Cells were washed and resuspended in artificial seawater (ASW) medium[62] at ~1x10^6 cells/mL for stable isotope labelling. Incubations were carried out in 20 ml of culture with 2 mM NaH$^{13}CO_3$ (Sigma-Aldrich Cat #: 372382) and vehicle DMSO or 10 nM concanamycin A (dissolved in DMSO) in 50 ml Erlenmeyer flasks in duplicate at 18C under ~500 μmol photons m^{-2} s^{-1} for 8h followed by addition of paraformaldehyde (3.7% final conc.). Controls included a culture without NaH$^{13}CO_3$ (but with unlabeled NaHCO$_3$) and a second culture where cells were fixed for 30 min and 2 mM NaH$^{13}CO_3$ subsequently added. All samples were pelleted and resuspended in silica-free ASW+10% hydrofluoric acid on a rotating incubator overnight to strip the cell wall in order to eliminate charging of Si during SIMS analysis. Triplicate washes in silica-free ASW were used to remove the acid before storage at 4C.

One ml of sample was filtered onto 0.2 μm pore size white polycarbonate filters (Millipore, Billerica, MA). After drying, filters were cut into ~1/8 sections and placed onto an analysis bullet using adhesive and conductive tabs (#16084–6, Ted Pella, Redding, California) and sputter coated with ~5 nm gold particles. A Cameca NanoSIMS 50 at Lawrence Livermore National Laboratory generated isotope images by rastering the primary $^{133}Cs^+$ ion beam (2 pA, ~150 nm diameter, 16 keV) across 35 × 35 μm analysis areas with 256 × 256 pixels and a dwell time of 1 ms/pixel, for 25 scans (cycles). Prior to ion collection, analysis areas were sputtered with 90 pA of Cs+ current to a depth of ~60 nm to achieve sputtering equilibrium and optimal ionization of intracellular isotopic material. Mass resolving power of the secondary ion mass spectrometer was tuned for ~7,000 (corrected units) to optimally collect quantitative secondary ion images for $^{12}C^{12}C–$ and $^{13}C^{12}C–$ on individual electron multipliers in pulse counting mode, as previously described.[63]

Image data generated from the NanoSIMS were processed and analyzed using L'Image. Following dead-time and image shift correction, $^{13}C^{12}C–/^{12}C^{12}C–$ ratio images were produced, revealing the level and location of ^{13}C fixation into biomass from $H^{13}CO_3^-$ in *T. pseudonana* cells treated with DMSO or concanamycin A. Regions of interest (ROIs) were drawn around cells based on their $^{12}C^{14}N$- and δ-^{13}C enrichment, which together indicated the centric biomass shape of each cell (Figure S2E). From each ROI, the $^{13}C^{12}C–/^{12}C^{12}C–$ ratios were extracted by cycle and averaged and then divided by two to calculate the $^{13}C/^{12}C$ ratio.[64] The $^{13}C/^{12}C$ ratios were then used to calculate net algal biomass produced from C fixation over the 8 h incubation period for each cell, called C_{net}.[63]

The NanoSIMS data were analyzed with Graphpad Prism 6 software and in RStudio. Values were checked for normality using Kolmogorov-Smirnov tests. Statistical comparisons of C-fixation data were performed with unpaired t-test with Welch's correction to compensate for different standard deviations between the controls and treatment.

^{14}C photosynthesis versus irradiance curves

Cultures of *T. pseudonana* grown in F/2 in 1 l bioreactor tubes bubbled with air and under continuous illumination by cool-white fluorescent lamps at ~100 μmol photons m^{-2} s^{-1} at 18C. The control (with vehicle DMSO) and 10 nM concanamycin A treated P-E incubations were performed over three days of batch culturing at standard DIC and low DIC relative to typical seawater levels (Table S2). Standard DIC conditions are at levels from unmodified culture medium while low DIC was reached by titrating cultures with 1M HCl and bubbling off excess CO_2 with air just prior to the incubations.

Photosynthesis-Irradiance (P-E) incubations were carried out by incubating cells in a modified ^{14}C bicarbonate incorporation technique described by Lewis and Smith.[65] Experiments were carried out in four custom P-E incubators maintained at 18°C and at 18 discreet irradiances ranging from 0 to 1678 μmol photons m^{-2} sec^{-1} illuminated by a 150W tungsten-halogen lamp. Discreet measurements of total photosynthetically available radiation (PAR, 400-700 nm) were taken with a Spherical Micro Quantum Sensor US-SQS (Heinz Walz, GmBH). For each P-E incubation, 100 μl of a 1 mCi NaH$^{14}CO_3$ (MP Biomedicals Cat #: MP0117441H2) solution was added to 25 ml of diatom culture samples to reach a final concentration of 4 μCi ml^{-1}. Spiked culture was aliquoted in 1 ml volumes into 21 pre-chilled 7 ml borosilicate glass scintillation vials. Eighteen of these vials were illuminated for 1 h in the P-E incubator while three remaining vials were immediately acidified with 150 μl of 12N HCl to drive off inorganic carbon and determine background activity for time-zero (T0) samples. Three total radioactivity (TA) samples were generated by combining 50 μl of spiked culture with 200 μl of phenylethylamine (Sigma-Aldrich) topped off with 5 ml of Ecolite(+) scintillation cocktail (MP Biomedicals) and capped immediately. Incubations were terminated after 1 h by switching off the lamps and adding 150 μl of 12N HCl to each vial. All acidified samples were allowed to exhaust un-fixed DIC overnight in a fume hood and topped off with 5 mL of Ecolite(+) and capped the next day for counting radioactivity on a Beckman Coulter LS6500 liquid scintillation counter.

Bulk carbon fixation rates (P_{bulk}; mg C l^{-1} hr^{-1}) were calculated from disintegrations per minute (DPM) by the equation:

$$P_{bulk} = (\mathrm{DPM_{sample}} / \mathrm{Vol_{sample}}) * (W * \mathrm{VolTA} / \mathrm{DPMTA}) * (1.05 / T)$$

Where $\mathrm{DPM_{sample}}$ is the T0 corrected activity per sample, $\mathrm{Vol_{sample}}$ is volume of culture per sample, W is the DIC concentration of the culture, $\mathrm{Vol_{TA}}$ is volume of culture in TA samples, $\mathrm{DPM_{TA}}$ is the activity per TA sample, 1.05 is the discrimination factor between ^{14}C and ^{12}C uptake, and T is the time duration of the incubations.

P-E curve fitting and calculation of VHA contribution

P_{bulk} was normalized by cell density to give cellular carbon fixation rates (P; fmol C cell^{-1} min^{-1}) and 18-point curves were fit with the equations by Platt et al.[66] using the Phytotools R-package.[55] Fitted curves were plotted from 0-1,600 μmol photons m^{-2} sec^{-1} and averaged amongst the respective conditions (Figure S4).

Paired two-tailed t-test were carried out on averages of the curve fitting parameters P_{max} (maximum cellular carbon fixation rate), α (initial slope), and E_k (half-saturation constant of photosynthesis) between control and concanamycin A treatments using Graphpad Prism 6. P-values showing statistical significance for each parameter are summarized in Table S2.

The contribution of VHA to P was calculated between control and concanamycin A treated average curve fits by the following equation:

$$\%\text{VHA contribution} = \left(\frac{P_{control} - P_{concA}}{P_{control}}\right) \times 100\%$$

QUANTIFICATION AND STATISTICAL ANALYSIS

Graphpad Prism was used to carry out paired two-sided t-tests of oxygen production and carbon fixation between control and VHA-inhibited samples, curve fitting on PAM rapid light curves for ETR_{PSII}, and two-way repeated measures ANOVA of oxygen production in the 2% CO_2 experiment, as well as to calculate mean and standard error mean values of replicate data. Phytotools R-package was used to fit and parameterize P versus E plots in RStudio. The NanoSIMS data were analyzed with Graphpad Prism 6 software and in RStudio. Values were checked for normality using Kolmogorov-Smirnov tests. Statistical comparisons of C-fixation data were performed with unpaired t-test with Welch's correction to compensate for different standard deviations between the controls and treatment. Carbonate chemistry in the cultures was calculated using CO2Sys_v2.1.[56]

Biological replicate number (n), standard error mean (SEM), confidence intervals (CI), and p-values are described in the figure captions or included within figures requiring statistical analysis. For bulk oxygen production and radioisotope carbon labeling experiments, a minimum sample size of 3 was selected for all measurements in order to carry out paired t-test analysis between control and treatment samples. For single-cell stable isotope carbon labeling experiments, sample size was based on availability of identifiable cells for analysis. Covariates in this study were between a given cell culture with vehicle DMSO or a pharmacological inhibitor dissolved in DMSO; this experimental design cannot be (and does not require to be) randomized.